RSC Applied Polymers

ROYAL SOCIETY OF CHEMISTRY

PAPER

View Article Online
View Journal | View Issue

Cite this: *RSC Appl. Polym.*, 2026, **4**, 568

Multifunctional flexible electrospun polydimethylsiloxane (ePDMS) membranes for soft robotics applications and photocatalytic conversion platforms

I. R. Reshma,[a,b,c] Gokula Nathan Kasinathan,[b] Akshay Tikoo,[d] Praveen Meduri,[d,e] Subha Narayan Rath *[b] and Shourya Dutta-Gupta *[c]

Functional polymers with tailored properties have been used for various applications and are expected to play a major role in the realization of flexible functional devices. In this study, we report the successful electrospinning of a hydrophobic polydimethylsiloxane (ePDMS) membrane, with the aid of a carrier polymer, polymethyl methacrylate (PMMA). Using the fabricated membranes, we demonstrate its applicability for the solvent-mediated trapping of objects and for enhancing photocatalytic activity. The shrinkage behavior of the ePDMS membrane in solvents such as IPA and EtOH is used to demonstrate their applications for creating membrane-based functional traps. Furthermore, the selective tuning of the permeability of the ePDMS membrane through gold sputtering on one side leads to the wrapping of the ePDMS membrane, and this was employed for plugging pores in tubes. The membranes also act as functional platforms for supporting enhanced photocatalytic conversion reactions. The ePDMS membranes act as oxygen diffusion membranes, eliminating the need for external oxygen purging. Our findings suggest that ePDMS membranes hold great potential for use in biomedical, sensor, electronic, and soft robotics fields. These insights pave the way for future research to fully explore the potential of ePDMS membranes.

Received 11th November 2025,
Accepted 22nd December 2025

DOI: 10.1039/d5lp00354g

rsc.li/rscapplpolym

1. Introduction

Multifunctional materials or smart materials, with their ability to perform a wide range of applications in response to some external stimuli, are highly effective and versatile in nature with the flexibility to be functionalized to meet various requirements. Smart materials have distinct advantages, such as selectivity, directness, immediacy, self-actuation, and transiency, and are experiencing significant growth in various sectors, particularly in medical and electronic applications.[1] The advent of advanced manufacturing techniques, such as electrospinning, has revolutionized the harnessing of stimuli-responsive materials for sensing, actuation, logic, and control applications by facilitating their micro- and nano structures, unlocking new horizons and unparalleled possibilities.[2] Such materials have found widespread use in areas such as catalysis,[3] sensors,[4] tissue engineering,[5] purification,[6] distillation[7] and flexible electronics.[8] Among these, there has been a growing demand for hydrophobic membranes with wettability exceeding 100°. Given its exceptional high water contact angle, these membranes are poised to make significant contributions to a range of applications, where traditional materials fall short.

Polydimethylsiloxane (PDMS) was selected as the base material in this study due to its exceptional flexibility, biocompatibility, hydrophobicity, and high gas permeability, all of which make it attractive for stretchable electronics, actuators, and membrane-based applications. However, PDMS is inherently difficult to electrospin due to its low viscosity and lack of chain entanglement. To overcome this, we utilized polymethyl methacrylate (PMMA) as a carrier polymer, enabling the successful electrospinning of PDMS into fibrous membranes with tunable mechanical and surface properties.[9] Various techniques like electrospinning, sol–gel method, plasma treatment, and lithography have been used to fabricate membranes

[a]*Center for Interdisciplinary Programme, Indian Institute of Technology Hyderabad, Kandi 502284, Telangana, India*
[b]*Regenerative Medicine and Stem Cell Laboratory (RMS), Department of Biomedical Engineering, Indian Institute of Technology Hyderabad, Kandi, Telangana 502284, India. E-mail: subharath@bme.iith.ac.in*
[c]*Nano-Optics And Devices Lab, Department of Materials Science and Metallurgical Engineering, Indian Institute of Technology Hyderabad, Kandi, Telangana 502284, India. E-mail: shourya@msme.iith.ac.in*
[d]*Energy Conversion And Storage Lab, Department of Chemical Engineering, Indian Institute of Technology Hyderabad, Kandi, Telangana 502284, India*
[e]*School of Chemical Engineering, Oklahoma State University, Stillwater, OK 74078, USA*

with control over different parameters, such as size, thickness, porosity, and permeability, which are essential for the diverse range of applications requiring multifunctionality. Electrospinning offers several advantages, such as a high degree of control over the morphology and surface properties of the resulting membranes, allowing for the tailoring of their properties to meet specific application requirements.[10] Additionally, electrospinning is a cost-effective method that can be easily scaled up for large-scale production, making it an attractive option for industrial applications.

In this process, a high voltage is applied to a polymer solution, causing it to form a droplet that elongates and stretches in a spiral motion to create a Taylor cone.[11] This solution is then deposited on a collector plate where it solidifies, resulting in the formation of highly detailed nanofibers. These advancements have the potential to revolutionize various fields, including biotechnology[12] and electronics.[11] Electrospun materials, commonly made of polymers, have been found to possess smart material properties through various engineering strategies, enabling them to respond intelligently to different stimuli.[12] Many electrospun membranes shrink under various conditions, such as temperature, pressure, solvent interaction, pH and many more.[13,14] This shrinkage of fibers under specific stimulus can be beneficial or detrimental, depending on the variety of applications involved. Gautam *et al.* successfully fabricated thermoresponsive nanofiber sheets by blending PNIPAAm, PMMA, and CQDs with a robustness of 30% (w/w) PNIPAAm concentration, which showed minimal dissolution when subjected to thermal stimuli. They achieved over 90% cell viability with HEK-293T cells and demonstrated efficient release of CQDs upon thermal stimulation, suggesting the potential of this nanofiber platform for on-demand cellular delivery applications.[15] Costa *et al.* experimentally proved that the introduction of additives, such as block copolymers of PEb-PEO, in the electrospun production of drug carriers significantly enhances controlled release, particularly in critical situations like extremely high pH, making it a promising approach for low-cost carriers with colonic action.[16] Fang *et al.* reported that shrinkage is more or less of an intrinsic property that can be found in almost all electrospun membranes, and he qualitatively explained the underlying mechanism of shrinkage of thermoplastic polyurethane (TPU) with the gradient pre-strain field hypothesis. According to the author's explanation, the non-uniform evaporation of the solvent during solidification results in varying pre-strain within the fiber. When solvent-induced shape recovery occurs, this pre-strained fiber experiences buckling and crimping, leading to the shrinking of the membrane.[14] Yuan *et al.*, on the other hand, investigated the shrinking behavior of electro-spun PLGA membranes in different liquids (PBS, EtOH, and blood) and discussed the underlying shrinking mechanism. According to the study, the shrinkage of the electrospun PLGA membranes is mainly governed by the polymer fibers glass transition, influenced by temperature and liquid environment. To mitigate this shrinkage, a heat stretching (HS) treatment strategy was introduced, effectively preserving the original membrane structure, and enhancing dimensional stability in PBS and blood environments. The shrinkage is caused by the molecular motion in fibers and the glass transition temperature affects the shrinkage.[13]

Materials exhibiting solvent-driven actuation have found extensive utility in soft robotics, where flexibility and responsiveness are critical. Likewise, porous, oxygen-permeable membranes are increasingly explored as scaffolds for enhanced photocatalysis due to their ability to facilitate gas diffusion and improve the reaction efficiency.[17]

In this article, we developed a novel method to achieve electrospun hydrophobic PDMS membranes by incorporating PMMA as a carrier polymer, and also to partially and selectively remove the carrier polymer. This addresses the intrinsic challenges of PDMS's low viscosity and molecular weight. In this study, we employed the electrospinning of PDMS using PMMA as a carrier polymer to overcome the intrinsic challenges of PDMS's low viscosity and chain entanglement, a strategy that has been previously reported in the literature.[18,19] Building upon these established methods, we introduce a sequential heat-treatment strategy to selectively remove most of the remaining PMMA carrier polymer while preserving the PDMS fibrous network. This stepwise treatment enables unique solvent-responsive shrinkage and folding behavior, which forms the basis for controlled permeability and functional trapping. The stepwise heat-treatment strategy effectively preserves the PDMS fibrous network while selectively partially removing PMMA, a method not previously reported, enabling unique stimuli-responsive behaviour and multifunctional applications, such as membranous traps, leak prevention, and enhanced photocatalytic H_2O_2 production. These electrospun nanofibrous membranes exhibit intensive solvent-responsive shrinkage in EtOH and isopropanol, enabling controlled permeability and functional trapping. In this work, we implement a sequential low-temperature heat-treatment protocol that selectively reduces the PMMA carrier while preserving a continuous ePDMS fibrous network, enabling robust solvent-driven shrinkage and folding. Building on this, we introduce asymmetric gold sputtering to program the local stiffness and surface energy of the membrane, which allows controlled folding for functional trapping and leak sealing. Finally, we demonstrate a previously unexplored use of ePDMS membranes as oxygen-permeable supports for enhanced photocatalytic H_2O_2 generation, eliminating the need for external oxygen bubbling. The membranes enhance the photocatalytic performance by acting as oxygen diffusion layers, utilizing their porous and hydrophobic nature to absorb atmospheric oxygen, thereby eliminating the need for the external oxygen bubbling commonly required in conventional photocatalysis setups. This multifunctional capability positions the membranes as a promising platform for advanced catalytic applications. To the best of our knowledge, this work is the first to demonstrate this application of the ePDMS membrane. We believe that our findings open new avenues for research and will inspire further investigations into the potential of ePDMS membranes for various applications in diverse fields.

2. Materials and methods

2.1. Materials

Polydimethylsiloxane (PDMS) Sylgard 184 Silicone Elastomer Base was purchased from Dow Corning India Pvt., Ltd. Polymethylmethacrylate (PMMA, molecular weight of 120 000), tetrahydrofuran (THF), ethanol (EtOH), isopropyl alcohol (IPA), acetone, dimethyl formamide (DMF), melamine, pluronic P123, nitro blue tetrazolium chloride (NBT), ammonium molybdate tetrahydrate, and potassium iodide (KI) were purchased from Sigma-Aldrich. Sulfuric acid (H_2SO_4; 98%) was purchased from Emsure. Gold target (99.99%) was purchased from Ted Pella, Inc. Deionized (DI) water with a resistivity of 18.2 Ω m at 25 °C was obtained using a Millipore Direct-Q3 UV system, and was used directly without any further modification for all experiments. All these chemicals were used as received without further purification.

2.2. Electrospinning PDMS-PMMA membranes

A composite solution of polydimethylsiloxane (PDMS) and the carrier polymer polymethylmethacrylate (PMMA) was prepared in a 4 : 1 ratio using a THF/DMF solvent mixture (2 : 1), based on previously reported methods with minor modifications.[19] Initially, the required amount of PMMA (18%) was measured and added to the solvent mixture. The mixture was then stirred for 2 h at 45 °C to ensure complete mixing. Once the PMMA was completely dissolved, it was allowed to cool. After cooling, a 10 : 1 mixture of PDMS curing agent and silicone polymer was measured and added to the composite solution containing PMMA. The resulting mixture was stirred for an additional hour to ensure complete homogenization. The composite solution was then loaded into a syringe for electrospinning. A distance of 15 cm between the tip of the needle and the collector plate containing aluminium foil was used in the electrospinning apparatus. A voltage of 12 kV was applied to the collector using a high-voltage power supply. A syringe pump with a flow rate of 0.5 mL h^{-1} was used for the electrospinning process, along with a 22 gauge blunt needle. The electrospinning was carried out to obtain membranes with the desired thickness and morphology of the fibers.

To ensure complete removal of residual THF and DMF after electrospinning, AS-ePDMS membranes were first dried in a desiccator at 50 °C for 24 h. Subsequently, the membranes were subjected to a stepwise heat-treatment protocol consisting of intermittent heating at 40 °C and 75 °C for a total duration of 12 h (1 h at 40 °C, followed by 2 h at 75 °C, repeated cyclically). This mild thermal treatment preferentially affects the less thermally stable PMMA domains, leading to their partial reduction while preserving the crosslinked PDMS network. The resulting membranes exhibit thinner fibers and smoother surface morphology, as well as attenuated PMMA-related signatures in SEM and Raman analyses, consistent with a significant decrease in the PMMA content. After heat treatment, the resultant PDMS (HT-ePDMS) & pristine PDMS (AS-PDMS) were imaged using a field emission scanning electron microscope (SEM, JEOL JSM 7800F) operated with a voltage of 10 kV and a working distance of 10 mm. Image J software was used to analyze the SEM images to determine the mean fiber diameter and its distribution. The wettability of the AS-ePDMS & HT-ePDMS membranes was evaluated using a contact angle goniometer (Kruss DSA25S Contact Angle Meter), and the sessile drop method. A confocal Raman system (Witec alpha 300R) was used to analyze the chemical properties of HT-ePDMS and ensure the reduction of the carrier polymer. The measurements utilized a grating with 600 lines per mm and a slit width of 300 mm. The spectrometer acquired the spectra with 3 accumulations and an exposure time of 10 seconds each.

2.3. Solvent mediated shrinking behavior of the HT-ePDMS membrane

Intermittent heat treatment at 40 °C and 75 °C over a period of 12 h was initially employed to reduce the PMMA content in the electrospun PDMS membranes. Post-treatment SEM images revealed a noticeable reduction in fiber diameter and smoother surface morphology, while Raman spectroscopy confirmed the attenuation of the PMMA-associated peaks, collectively indicating the effective reduction of a substantial portion of the carrier polymer. To further reduce any residual PMMA, the heat-treated membranes were subjected to additional solvent washing steps. These treatments were intended to dissolve and extract a fraction of the PMMA domains that might remain entrapped within the PDMS network after thermal processing, thereby lowering the PMMA content and yielding a more PDMS-rich membrane for subsequent analyses. Each experiment utilized 1.2 × 1.2 cm^2 area ePDMS membranes. To observe the shrinking behavior, the HT-ePDMS membrane was immersed in 3.5 mL of different solvents, namely EtOH, IPA (IPA), and acetone, using a Petri dish. A video was recorded at a frame rate of 30 frames per seconds (fps) for each case, and the extracted images were subsequently analyzed using ImageJ software. Additionally, gold was sputtered onto the membrane for different time intervals (15 seconds, 30 seconds, and 60 seconds) using a tabletop sputtering system (Quorum Q150RS plus) to control the mechanical stiffness of the HT-ePDMS membrane and its pore size.

2.4. Functional traps using HT-ePDMS

To create functional traps using HT-ePDMS, a stencil was made by cutting a transparent acrylic plexiglass into a 1.5 cm × 1.5 cm cross shape, with a center square space covered. Next, we positioned the stencil on top of the membrane and proceeded to perform gold sputtering on one side of the membrane. On the opposite side, we conducted full sputtering, including the hole. Following the completion of the sputtering process, we meticulously cut the membrane using a sharp blade, adhering to the patterned stencil shape. The resultant cross-shaped membrane was further characterized and analysed to evaluate its shrinking and folding properties, and the patterned traps were immersed in EtOH (3 mL) to observe and monitor any shape changes.

2.5. Leakage prevention using HT-ePDMS membranes

A PTFE tube with a length of 5 cm and diameter of 0.5 cm was used. First, a hole was created in the PTFE tube to artificially create a leakage point. Using a syringe, 1 mM solution of Rhodamine 6G (R6G) dye was introduced into one end of the tube. To demonstrate leakage prevention using HT-ePDMS, a tube was placed above the gold-sputtered membrane, which was immersed in 3 mL EtOH in a plate. Within a few seconds, the membrane folded tightly around the central holed tube, and R6G was again passed through one end of the tube with the help of a syringe.

2.6. Synthesis of mpg C_3N_4

5 g of melamine and 1 g of pluronic P123 were dispersed in 100 mL of DI water.[20] The solution was heated under reflux at 100 °C for 1 h. 3 mL of sulfuric acid (H_2SO_4 : H_2O 1 : 1 v/v) was added to the solution to obtain a white precipitate. The solution was filtered, and the filter cake was dried overnight at 80 °C. Finally, the dried powder (mpg C_3N_4) was calcined at 550 °C under air for 4 h.

2.7. H_2O_2 photocatalytic synthesis using the ePDMS platform

To prepare the catalyst ink, 25 mg of mpg-C_3N_4 powder was added to 10 mL of EtOH, followed by ultrasonication for 10 minutes to achieve a well-dispersed suspension. Then, 1 mL (2.5 mg catalyst loading) of this ink was drop-cast onto a PDMS membrane sheet (2.5 cm × 2.5 cm) and allowed to dry at ambient temperature for 24 h. The membrane was subsequently floated on water with the coated side facing down to establish a solid–liquid interface, while the opposite side remained exposed to the atmosphere, forming a solid–gas interface (Fig. 5a). A 150 W Xenon (Xe) arc lamp served as the light source, and the experiment ran for 5 h. Afterward, a 1 mL sample was collected, to which 50 μL of 0.1 M ammonium molybdate tetrahydrate, 2 mL of 0.1 M KI, and 1 mL of DI water were added, producing a yellow solution. This solution's absorbance was then measured using a UV-vis spectrophotometer (LAB INDIA UV 3200). All photocatalytic experiments were repeated three times independently (n = 3), and the data are presented as mean ± standard deviation, with error bars shown in Fig. 5.

3. Results and discussion

3.1. Effect of heat treatment on the characteristics of ePDMS

Fig. 1(a) shows the electrospinning process employed for the PDMS/PMMA solution. The solution was prepared by mixing PDMS with a 10 : 1 ratio of elastomer to curing agent and 18% PMMA with an average molecular weight of 120 000. The PMMA was previously prepared using a solvent combination of 2 : 1 THF to DMF, which was selected based on the solubility parameter.[21] THF closely matches the solubility parameter of PDMS and PMMA, while DMF acted as a cosolvent to prevent excess volatilization of THF during electrospinning. Fig. 1(b) displays scanning electron microscopy (SEM) micrographs of the (AS-ePDMS), revealing a crowded morphology with thick fibers and a layer of flocs or roughness over the surface of the membrane. To ensure the removal of residual THF and DMF solvents after electrospinning, AS-ePDMS membranes were subjected to vacuum drying at 50 °C for 12 h, followed by 40 °C and 75 °C intermittent heat treatment before Raman and SEM characterization. This step ensures that the observed morphological and chemical changes are due to PMMA reduction, rather than residual solvent volatilisation. In contrast, the SEM micrographs after heat treatment (HT-PDMS) in Fig. 1(c) exhibit a smooth fiber layer and thinner fiber diameter compared to AS-ePDMA. The fiber diameter of the AS- and HT-ePDMS membranes was analyzed using ImageJ soft-

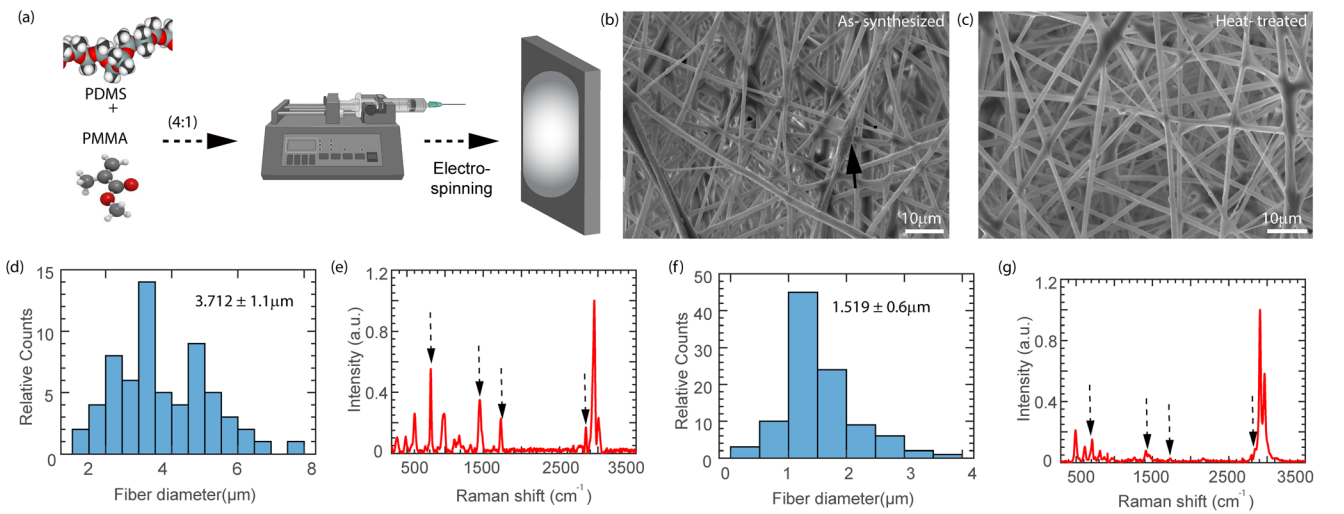

Fig. 1 Electrospinning of PDMS (ePDMS). (a) Schematic showing the electrospinning of PDMS using PMMA as the carrier polymer. (b) SEM micrograph of the AS-ePDMS. (c) SEM micrograph of the HT-ePDMS membranes. Mean fiber diameter of the (d) AS-ePDMS membranes and (f) HT-ePDMS. Raman analysis of the ePDMS membranes: (e) AS-ePDMS, (g) HT-ePDMS. The arrows in (e) and (g) correspond to the Raman spectrum of PMMA.

ware. AS-ePDMS exhibited a diameter ranging from 0.5 to 8 μm and an average fiber diameter of 3.7 ± 1 μm (Fig. 1(d)), while HT-ePDMS showed a diameter varying from 0.5 to 3.5 μm and an average fiber diameter of 1.5 ± 0.6 μm (Fig. 1(f)). The SEM micrographs and fiber diameter analysis provide indirect evidence that the heat treatment substantially reduces the PMMA content in the membrane, which was used as the carrier polymer. The selective reduction of PMMA is facilitated by its lower thermal stability compared to PDMS; heating at 40 °C followed by 75 °C softens and partially volatilizes PMMA chains, while the crosslinked PDMS network remains intact. This process leads to thinner fibers and a smoother surface morphology, as observed in the SEM images, consistent with a PDMS-rich fibrous network with reduced PMMA content (Fig. S4). We employed Raman spectroscopy to compare the characteristic Raman peaks of the AS- and HT-ePDMS membranes with those of pristine PDMS and PMMA (Fig. S1).[22] Fig. 1(e) and (g) represent the Raman peaks of the AS- and HT-ePDMS membranes, respectively.[23] In Fig. 1e (as-electrospun fibers), the arrows highlight the prominent PMMA-related peaks and bands where the PDMS and PMMA contributions overlap. After the two-step thermal treatment, the corresponding spectrum in Fig. 1g shows that the relative intensities of these PMMA-associated bands are substantially reduced once normalized to the maximum PDMS peak, whereas the PDMS bands are preserved. This decrease in the PMMA peak intensity, together with the reduction in the fiber diameter after heating, indicates a significant depletion of the PMMA phase while maintaining the PDMS network, which we identify as the structural basis for the characteristic shrinkage and folding behaviour of the HT-ePDMS membranes selected for further experiments[24] (Fig. S4). The AS PDMS–PMMA (AS-ePDMS) membrane displays prominent FTIR absorption bands corresponding to both PMMA and PDMS. The peaks at ~1728 cm^{-1} (C═O stretching), 1260 cm^{-1} and 1144 cm^{-1} (C–O–C asymmetric and symmetric stretching), 1454 cm^{-1} (CH_2 bending), and the broad 2962–2858 cm^{-1} (C–H stretching) confirmed the presence of PMMA within the composite matrix. In addition, PDMS characteristic peaks were observed at ~1060 cm^{-1} (Si–O–Si asymmetric stretching), 802 cm^{-1} (Si–C stretching), and 760 cm^{-1} (CH_3 rocking), indicating successful blending of both polymers (Fig. S5).[24] After sequential heat treatment at 45 °C and 70 °C, the intensity of the PMMA-associated peaks markedly decreased, while the PDMS peaks became sharper and more prominent, confirming the effective reduction of PMMA and retention of the PDMS network. This transformation can be attributed to enhanced chain mobility and phase segregation at mild heating, which facilitates PMMA diffusion and extraction from the fiber matrix without thermal degradation.[25] The process preserves the thermally stable PDMS backbone and results in a purified, elastic ePDMS membrane with smoother fiber morphology and reduced fiber diameter.[26]

PDMS is a hydrophobic material, typically exhibiting a water contact angle greater than 90° and close to 120°, which indicates its resistance to wetting by water.[27] Even after the selective reduction of PMMA, the membranes retained their high hydrophobicity, as confirmed by water contact angle measurements (Fig. S2). The AS-ePDMS membrane exhibited a contact angle of 126° ± 0.7°, while the HT-ePDMS membrane showed a contact angle of 125.3° ± 0.95°, indicating that the heat treatment does not compromise the intrinsic hydrophobicity of the PDMS fibers.[28] This preservation of surface properties is crucial for applications where water repellency and controlled solvent interaction are required, such as in solvent-induced actuation and photocatalytic processes. While the electrospinning of PDMS using PMMA as a carrier polymer has been reported previously,[18,19] the present work focuses on the downstream applications of the HT-ePDMS membranes, including solvent-responsive actuation and photocatalytic H_2O_2 generation. This hydrophobic property makes it suitable for applications and allows for selective tuning of the membrane through various processes. This tunability enhances its suitability for a wide range of applications, including fluid separation,[29] barrier systems,[30] protective coatings,[31] sensors[32] and in biomedical applications.[33,34] Therefore, our results demonstrate that the employed heat treatment procedure effectively reduces PMMA from the AS-ePDMS membranes, resulting in a decrease in fiber diameter and a smoother fiber layer morphology. The effective reduction of PMMA from the membrane was also confirmed through Raman analysis. In all the subsequent experiments, we use HT-ePDMS to demonstrate the stimuli-based response of these membranes. While our study provides evidence of PMMA reduction through SEM, FTIR, and Raman analyses, we acknowledge that a detailed mechanistic investigation was not conducted. However, existing literature offers insights into the thermal degradation of PMMA. For instance, studies have shown that PMMA undergoes thermal degradation upon heating, leading to the volatilization of its components without affecting the thermally stable PDMS network. This supports the inference that the sequential heat treatment employed in our study effectively reduces PMMA while preserving the PDMS structure.[35] While the current study confirms the selective reduction of PMMA and preservation of the PDMS network, a detailed mechanistic investigation into the thermal degradation pathway would further elucidate the underlying physicochemical transformations. This remains a limitation of the present work and will be addressed in future studies.

3.2. Shrinking behavior of HT-ePDMS

The impact of solvent interactions on the mechanical property, porosity, and structural stability of electrospun nanofiber membranes is critical in determining the efficacy of fiber welding and inter-fiber bonding. These properties affect the membranes' suitability for a variety of applications in fields, such as energy storage, environmental remediation, and biomedical engineering.[36] Previous studies have shown that the shrinkage mechanism of amorphous materials can be triggered by various parameters, such as solvent interaction, glass transition temperature, heat, stress–strain gradient, and others.[13] These mechanisms can be used for optimizing the

fiber properties required for various functional applications. In this study, we study the shrinkage of the HT-ePDMS substrates in various solvents and subsequently control the permeability of the membranes for different functional applications.[13] Three different common solvents, IPA, EtOH and acetone, were used to understand the stability and shrinkage response of the HT-ePDMS membranes.[37]

Fig. 2(a) shows the schematic of the HT-ePDMS membrane shrinkage in two different solvents (isopropyl IPA & EtOH) as a function of the immersion time. Fig. 2(b) and (c) show the shrinkage of the HT-ePDMS membrane in EtOH and IPA, respectively. These images were extracted from videos recorded at a rate of 30 frames per second. The HT-ePDMS tends to shrink in IPA (Video S1) and EtOH (Video S2) while in the acetone, HT-ePDMS tends to degrade and disintegrate (Video S3). As observed in Fig. 2(b), the shrinkage of the HT-ePDMS membrane in EtOH was faster compared to the shrinkage rate in IPA, as depicted in Fig. 2(c). Fig. 2(d) and (e) show the SEM micrographs of the HT-ePDMS membranes after the shrinkage in EtOH and IPA, respectively. Unlike Fig. 1(b) and (c), these micrographs depict a non-uniform, curved morphology of fibers, and membrane breakage at some parts was also observed. Additionally, a crimped morphology is seen, confirming the buckling due to the gradient pre-strain field in the cross-section of the fibers.[14] We conducted a chemical characterization using Raman spectroscopy to verify if any chemical changes occurred due to immersion of HT-ePDMS in the solvent. Fig. 2(g) displays the Raman peak comparison of the shrunken HT-ePDMS membrane in IPA (red) and EtOH (blue). The IPA- and EtOH-immersed HT-ePDMS membranes show the same peaks as in Fig. 1(g), demonstrating no major changes in the chemical signatures of the HT-ePDMS membranes. To confirm the shrinkage percentage, we extracted the relative area of the membrane as a function of time. The relative area is defined as the ratio of the area of the ePDMS membrane at time t divided by the area of HT-ePDMS membrane at $t = 0$ s. Fig. 2(f) shows the relative area as a function of time on immersion of HT-ePDMS membranes in IPA and EtOH. The data presented represent the mean values from three independent experiments ($n = 3$), with error bars indicating the standard deviation. Reproducibility of the shrinkage behavior was confirmed through repeated trials, which consistently demonstrated similar trends for HT-ePDMS membranes in both ethanol and isopropanol. This reproducibility can be attributed to the uniform fiber morphology and crosslink density of the heat-treated ePDMS membranes, which govern solvent absorption and swelling. Additionally, the solvent-membrane interactions are dominated by the polarity and solubility parameters of the liquids relative to PDMS, leading to predictable and repeatable shrinkage rates. The relative area reduction and calculated half-life values remained comparable across multiple measurements, confirming that the solvent-mediated shrinkage of HT-ePDMS is both reliable and mechanically controlled. Although HT-ePDMS shrank faster in EtOH, more

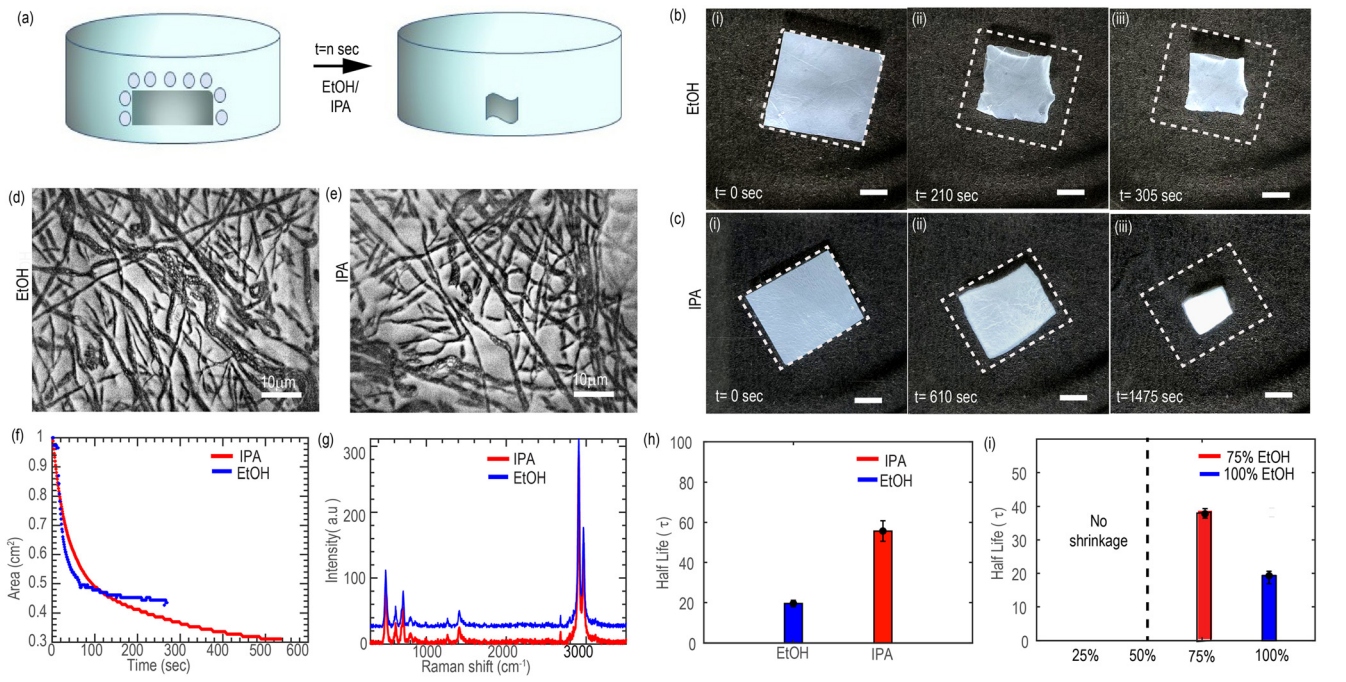

Fig. 2 Shrinking behavior of HT-ePDMS. (a) Schematic of the ePDMS membrane shrinkage in two different solvents (isopropyl IPA & EtOH) as a function of the immersion time. (b) Images of the HT-ePDMS membranes immersed in EtOH at different times. (c) Images of the HT-ePDMS membranes immersed in IPA at different times. SEM images of the HT-ePDMS membranes after shrinking in both (d) IPA and (e) EtOH. (f) Area of the HT-ePDMS as a function of time after immersion in EtOH and IPA. (g) Raman spectra of the HT-ePDMS membranes after shrinkage in both solvents (IPA & EtOH). (h) Half-life (τ) of the HT-ePDMS membrane shrinkage in both IPA and EtOH extracted from the images. (i) Half-life (τ) comparison of the ePDMS shrinkage in different concentrations (0%, 25%, 50%, 75% & 100%) of EtOH.

shrinkage was observed in the IPA-treated membranes. We calculated the shrinkage rates using the formula $s = ((A_0 - A)/A_0) \times 100$, where A_0 is the initial area (t = 0 s) and A is the final area. The shrinkage percentage for the normalized area was found to be 58% and 70% for EtOH and IPA until 600 seconds, respectively.

An exponential curve, $A_{rel} = C_1 \times e^{(-x/t1)} + C_2$, was fitted to the time-dependent relative area of the membrane to understand its decay constant and half-life (Fig. S3). The decay constant and half-life (tau/τ) for the HT-ePDMS membrane in EtOH were found out to be 0.03 and 17 ± 0.4 seconds, respectively. Here, tau/τ represents the time constant in an exponential decay or a growth process. Similarly, the decay constant and half-life (τ) for the HT-ePDMS membrane in IPA were found out to be 0.01 and 58.5 ± 0.6 seconds, respectively, which can be further observed from Fig. 2(h). The decay constant and half-life varies on interacting with different solvents with respect to time. Therefore, it is possible to tune the shrinkage rates by a judicious choice of the immersion medium.

Fig. 2(i) shows the extracted half-life of the HT-ePDMS membranes in different concentrations of EtOH in an EtOH–water solution. It is evident that the HT-ePDMS membrane in 100% and 75% EtOH shows a half-life of 17 ± 0.4 and 36 ± 0.5 seconds, respectively. On the other hand, immersion of the HT-ePDMS membrane in 50% and 25% EtOH did not exhibit any shrinkage. The electrospun PDMS membrane is known for its high stability, low surface energy, and resistance to swelling by solvents. The lack of shrinkage observed when exposed to 50% and 25% EtOH may be due to the weak interaction between the PDMS membrane and EtOH molecules. EtOH is a polar solvent that can interact with the PDMS surface through hydrogen bonding and van der Waals forces. However, at lower concentrations, these interactions are limited, resulting in minimal changes to the membrane structure. At higher concentrations, the solubility parameter of EtOH becomes closer to that of PDMS, allowing the EtOH molecules to penetrate the polymer network more easily and causing the membrane to swell or deform. This behavior is explained by the concept of free volume, which is the space between polymer chains that is not occupied by atoms or molecules. At low EtOH concentrations, there is less free volume available for the EtOH molecules to occupy, limiting the extent of swelling or deformation.[38] At higher concentrations, the increased availability of free volume allows the EtOH molecules to cause more significant changes to the membrane structure.[39]

A limitation of the current study is that, with the present experimental setup, electrospinning PDMS without a carrier polymer is challenging. Therefore, direct PDMS-only controls could not be included. Future work could explore alternative fabrication strategies to produce pure PDMS nanofibers and further validate the intrinsic behavior of PDMS in such membranes.

3.3. Controlling permeability of HT-ePDMS

Controlling the permeability of electrospun nanofiber membranes is essential to maximising their performance in a variety of applications, such as filtration,[40] wound treatment, and tissue engineering.[41] Through precise measurement and regulation of air permeability, scientists can ensure the effective passage of gases or liquids over or through the membrane, therefore augmenting its appropriateness for certain industrial or biological applications. Comprehending the correlation among fibre form, surface characteristics, and permeability facilitates the creation of nanofiber membranes customised to fulfil the demands of diverse uses, therefore propelling the domain of nanotechnology and its pragmatic implementations in medicine and other domains.[40,41] The deposition of gold on ePDMS membranes alters their surface energy of the coated surface, its mechanical stiffness potentially leading to the different stiffnesses of the coated and uncoated surfaces. Furthermore, surface roughness or patterning could alter how the membrane interacts with the solvent by tuning the permeability through pore size control.

Fig. 3(a) shows a schematic of the proposed method for controlling the interaction of the HT-ePDMS membrane with the solvents. By selectively varying the time and depositing a layer of gold with known thickness, it is possible to controllably tune the solvent–surface interaction. In particular, the gold layer's thickness can alter the ePDMS membranes' stiffness and also modify the surface energy of the coated interface. The membranes were coated with three different thicknesses of the gold layer *via* tuning the deposition times (15 seconds, 30 seconds, or 1 min). The nominal thickness of the gold layer are around 10 nm, 20 nm and 40 nm, respectively, for the three deposition times. For the 15 seconds deposition, the gold islands are formed on the HT-ePDMS membranes, whereas a continuous layer of gold is deposited for the 30 seconds and 60 seconds deposition times. It should be noted that in all these samples, only one surface of the HT-ePDMS membrane is coated with gold. Fig. 3(b)–(d) show the images of the gold-coated HT-ePDMS membrane at different time points on immersion in EtOH. The membrane has been immersed such that the uncoated surface is on the top and the gold coated surface is in contact with the Petri dish.

In the case of 15-second sputtering, the formation of gold clusters or islands results in voids that allow the solvent to interact with the membrane, causing significant shrinkage. For the 30-second sputtered membrane, an optimal gold thickness forms, reducing solvent–membrane interaction and allowing for complete fold-back. However, with 60 seconds of sputtering, the gold layer becomes too thick, limiting the membrane's ability to fully fold back. A shrinkage study on these modified membranes using EtOH was conducted. One side of each membrane was coated with gold for different sputtering durations (15, 30, and 60 seconds), and the membranes were exposed to EtOH. Interestingly, the membrane sputtered for 15 seconds showed pronounced shrinkage (Video S4), while the 30-second sputtered membrane fully folded back (Video S5). The 60-second sputtered membrane also exhibited folding, but it did not fold back completely (Video S6).

Overall, gold deposition likely alters the mechanical properties of the membrane, making it more flexible or deformable. The 30-second sputtered ePDMS membrane exhibited

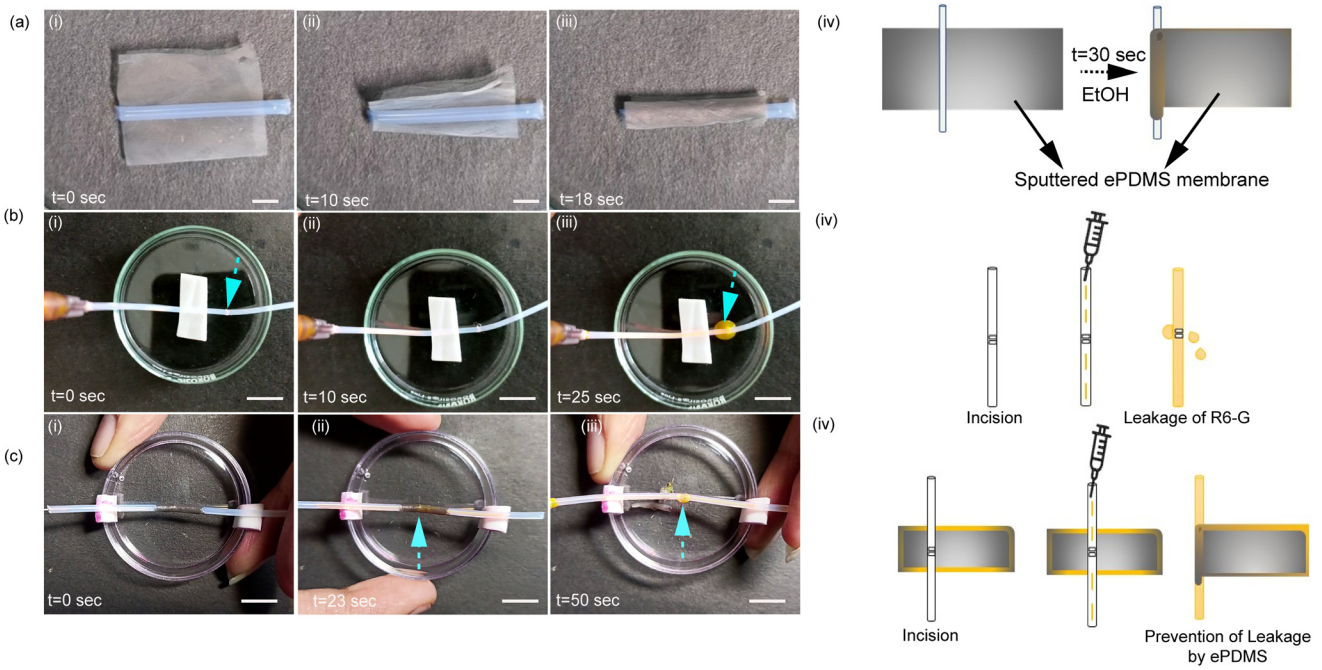

Fig. 3 Controlled shrinking and folding through selective deposition. (a) Schematic of the effect of deposition of gold in ePDMS membranes by sputtering before and after immersion in EtOH at different time periods. Effect of the ePDMS membrane at different gold sputtering times at (b) sputtering time = 15 seconds, (c) sputtering time = 30 seconds, and (d) sputtering time = 60 seconds [each frame extracted from the process at each second]. (b)(iv) Represents the rolling effect of the gold-sputtered ePDMS membrane in EtOH at time, $t = n$ seconds. Schematic representation of the effect of the ePDMS membrane in EtOH at two different sputtering times: (c)(iv) sputtering time = 15 seconds, (d)(iv) sputtering time = 30 seconds/1 min.

the most efficient folding, and the sputtering time was selected for further experiments. The folding behavior appears to result from changes in surface energy and mechanical properties induced by gold sputtering, including variations in stiffness and elasticity, which affect the membrane's response to external stimuli like solvents. Combining HT-ePDMS with controlled solvent actuation and gold sputtering creates a multifunctional platform, enabling tunable folding and practical applications such as membranous traps and leak prevention. Further experiments are needed to fully understand the mechanism and to tailor the membrane's properties for specific applications.

3.4. Functional traps using HT-ePDMS

We use the selectively coated HT-ePDMS membranes for demonstrating the potential functional applications of these membranes. As demonstrated in the previous sections, the fabricated HT-ePDMS membranes demonstrate a unique shrinking and folding behavior in the presence of EtOH, making them ideal for use in membranous trap setups for a variety of fields, including sensors, cell trapping, soft robotics, wearable electronics, *etc*.

We developed two types of gold sputtering on the same membrane, each cut into a cross shape. The first type, referred to as FLAP F, was fully coated with gold on one side (bottom side), while the second type, FLAP H, had its four flaps gold-sputtered, leaving the center portion unsputtered on the upper side. In our experimental setup, we placed the FLAP F membrane in contact with a Petri dish containing EtOH. Meanwhile, the FLAP H membrane was positioned with its gold-sputtered flaps facing upwards (Fig. S8 in the SI). Our results revealed that when exposed to EtOH, the gold-sputtered flaps of the FLAP H membrane behaved like a Venus flytrap, folding inward towards the unsputtered center region (Fig. S9 and Video S7). This folding mechanism demonstrates potential for applications in areas such as cell trapping, soft robotics, flexible wearable electronics, sensors, and more. These findings suggest that these engineered ePDMS membranes offer significant versatility and promise for various functional applications. Self-folding smart materials, such as self-folding polymer films and electrospun fiber mats, represent a cutting-edge approach in tissue engineering, particularly in vascular and nerve tissue regeneration. By harnessing their unique properties, these materials can create complex 3D structures with tailored porosity, closely resembling the intricate architecture of native tissues. This capability facilitates improved cell infiltration and vascularization, critical for fostering nutrient transport and waste removal in engineered tissues. Furthermore, the controlled alignment of fibers in electrospun mats mimics the anisotropic nature of natural extracellular matrices, offering guidance cues for nerve regeneration within conduits.[42] The stimuli-responsive folding behavior of the gold-sputtered HT-ePDMS membranes mimics actuation-like movements without external mechanical input,

making them ideal candidates for soft robotic applications. In particular, their ability to fold reversibly and shrink and wrap in response to ethanol demonstrates a controllable deformation mechanism that could be engineered into autonomous soft grippers or self-sealing actuators. Such a solvent-triggered response aligns well with the design principles of soft robotics, where materials are expected to perform complex tasks through simple stimuli. HT-ePDMS membranes, prepared *via* sequential thermal treatment, provide a versatile platform for soft robotics, self-sealing structures, and enhanced photocatalysis, extending the utility of electrospun PDMS beyond previous reports. These findings highlight the potential of our membrane system to serve as building blocks for next-generation soft robotic devices, particularly in biomedical and microfluidic environments.

Fig. 4a illustrates the folding back of a 30-second sputtered ePDMS membrane in EtOH when a 0.2 mm PTFE tube is placed over it. The membrane holds the tube tightly and wraps around it as it folds (Video S8). Fig. 4a(i)–(iii) depict various frames extracted from the experimental video. Fig. 4a(iv) is the schematic illustration of the experimental setup. Also, 1 min folding back was performed (Fig. S10) (Video S9).

To support our findings, we modified the experiment as shown in Fig. 4(b), where a center hole was punctured in the middle of the tube, and diluted Rhodamine 6G dye was injected into one end to detect leakage. As expected, the punctured tube exhibited leakage, as shown in Fig. 4(b)(iii). The blue arrows represent the punctured areas of the PTFE tube. Fig. 4(b)(iii) clearly shows the leakage (Video S10). In summary, our study highlights the functional applications of our engineered ePDMS membranes, which exhibit excellent folding behavior in the presence of EtOH. These findings offer exciting opportunities for the development of membranous trap setups for various fields, including cell trapping, soft robotics, wearable electronics, and more. Additionally, our experiments demonstrate the membranes' ability to tightly hold and wrap around a PTFE tube, further indicating their potential use in leakage studies. In order to evaluate the folding capabilities of the 30-second sputtered ePDMS membrane on a tube, we conducted a repetition of the experiment depicted in Fig. 4(c). Specifically, we positioned the centered hole tube over the membrane while it was immersed in EtOH. To our surprise, the membrane successfully prevented any leakage as it wrapped itself around the hole. To verify this

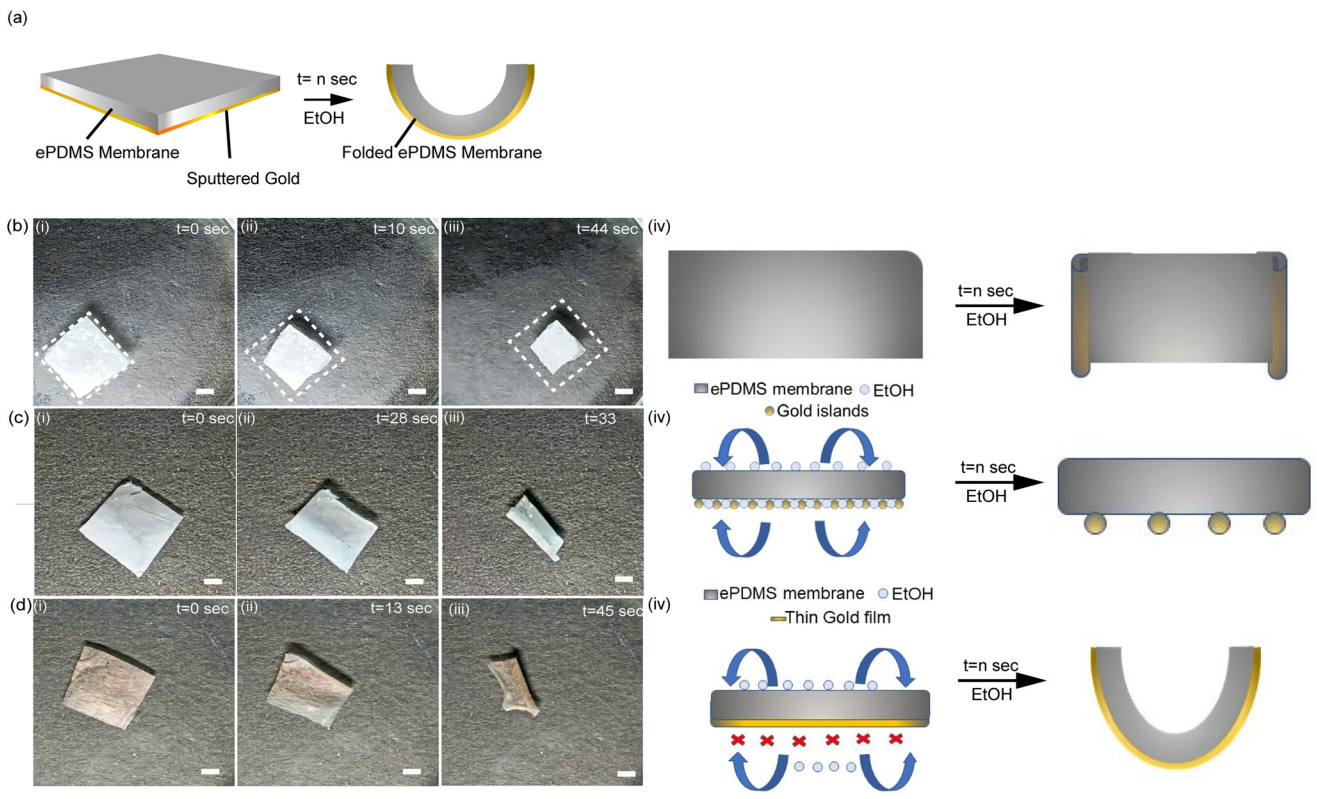

Fig. 4 Patterning of ePDMS membranes for functional traps. (a)(i)–(iii) Sequence of images showing the bottom-side gold-sputtered ePDMS membrane with a tube placed on it, immersed in EtOH (EtOH) over a total process duration of 18 seconds (each frame corresponds to a specific time point in seconds). (a)(iv) General representation of the gold-sputtered ePDMS membrane at a specific time ($t = n$ seconds) in EtOH, with a tube placed on it. (b)(i)–(iii) Experimental demonstration of a tube with an incision where dye-containing solution is injected, leading to dye leakage through the incision. (b)(iv) General schematic of the leakage from the incision after dye injection. (c)(i)–(iii) Experimental results showing that when the ePDMS membrane is tightly wrapped around the tube, no dye leakage occurs, but leakage starts once the membrane is removed. (c)(iv) General schematic of the leakage experiment, with the ePDMS membrane tightly wrapped around the incision site on the tube.

phenomenon, we removed the membrane and performed the experiment once again, which resulted in leakage as before. Fig. 4(c)(i) illustrates the gold-sputtered ePDMS membrane wrapped around the punctured tube at time t = 0 s, while Fig. 4(c)(ii) highlights the tightly wrapped, leak-free portion of the membrane. To verify this phenomenon, we removed the membrane and repeated the experiment once again, which resulted in leakage as before. Fig. 4(c)(i) illustrates the gold-sputtered ePDMS membrane wrapped around the punctured tube at time t = 0 s, while Fig. 4(c)(ii) highlights the tightly wrapped, leak-free portion of the membrane. Finally, Fig. 4(c)(iii) demonstrates the leakage that occurs once the membrane is removed (Video S11). To further assess the reliability of this sealing behavior, we conducted repeated swelling and shrinkage cycles to evaluate the basic durability. Although systematic fatigue testing and long-term solvent exposure studies were beyond the scope of this work, the gold-sputtered HT-ePDMS membrane retained its folding behavior and sealing capability over five consecutive ethanol-triggered cycles. In each case, it consistently formed a tight seal around the punctured PTFE tube. These trials were performed manually under controlled laboratory conditions and showed no observable degradation in performance. Extensive quantitative fatigue testing and prolonged solvent exposure studies will be necessary to validate the long-term applicability of these membranes in reusable or load-bearing biomedical systems.

This adaptive behavior, particularly the ethanol-triggered self-folding and wrapping around objects such as PTFE tubes, demonstrates actuation-like functionality that is highly relevant to soft robotics. Materials capable of undergoing reversible, environment-triggered deformation without mechanical interfaces are of increasing interest in the field, especially for developing soft grippers, actuating flaps, and self-sealing structures. The interface-free, stiffness-gradient architecture of our electrospun PDMS membranes supports localized deformation and controlled motion, features that align with recent biomimetic design strategies in soft robotics. Although our current study does not include a full robotic integration, these preliminary demonstrations of solvent-responsive movement and conformal wrapping offer foundational insight into their potential for such applications. Our findings are in agreement with previous reports on biomimetic polymeric systems engineered for responsive movement and mechanical adaptability in soft robotic platforms. Given these unique features, the membrane holds great promise for a variety of biomedical applications, including drug delivery systems, nerve conduits, and wound healing, among others.[43,44]

3.5 HT-ePDMS as a functional platform for photocatalytic conversion

In previous sections, we discussed the solvent-mediated shrinkage of HT-ePDMS membranes, leveraging this property for the targeted trapping and plugging of leaks. Here, we focused on the hydrophobicity and gas permeability of HT-ePDMS membranes, which enhance photocatalytic activity in the production of H_2O_2.

Photocatalytic H_2O_2 synthesis was conducted in triplicate with C_3N_4 coated on a PDMS membrane at ambient temperature and pressure in the presence of light for 5 h (M + C + L). To confirm the catalyst presence on the ePDMS membrane, a SEM micrograph was obtained, as shown in Fig. 5(b). Elemental dispersion spectroscopy (EDS) was also done to further validate the presence of C_3N_4 coated on HT-ePDMS (three different spots in the same membrane), as shown in SI Fig. S11. Control experiments included a membrane-free setup (where 20 mg of photocatalyst was dispersed in 20 mL of water) (C + L) and a setup in the absence of light (M + C − L) and one without both membrane and light (C − L). The absence of significant H_2O_2 production under dark conditions indicates that H_2O_2 formation is not due to electrocatalysis (Fig. 5(c)). The M + C + L system achieved a high yield of 52.5 μM H_2O_2 over 5 h, compared to 18.3 μM H_2O_2 in the C + L setup, despite using eight times less catalyst (2.5 mg for M + C + L *vs.* 20 mg for C + L). The performance of our system is comparable with that reported in the existing literature, although some modified g-C_3N_4 systems have demonstrated higher efficiencies. For instance, a study on the Pt/g-C_3N_4 Schottky junction by Nie *et al.* reported a H_2O_2 yield of ~13 μM with pure g-C_3N_4 without sacrificial agents under visible-light irradiation, and the yield of ~32 μM highlighted the enhancement due to Pt nanoparticle deposition.[45] Another research by Peng *et al.* achieved ~30 μM with pure g-C_3N_4 and ~140 μM H_2O_2 using CoP-loaded g-C_3N_4 wing to enhanced photogenerated electron transfer and inhibited recombination of electron–hole pairs. This performance difference can be attributed to the distinct oxygen delivery mechanisms. Atmospheric O_2 readily reaches the catalyst surface in the membrane setup, creating a consistent supply of oxygen.[46] The membrane's supply porosity facilitates O_2 diffusion to the reaction interface, supporting a high density of excited electrons that react to produce H_2O_2, effectively reducing electron–hole recombination. In contrast, atmospheric O_2 slowly diffuses through water to reach the catalyst in the dispersed setup, limiting the overall reaction rate.[47] The reactions follow zero-order kinetics, with the H_2O_2 concentration increasing linearly over time. The formation and degradation of H_2O_2 typically follow zero and first-order kinetics, respectively.[48] As the concentration of H_2O_2 is very low, it can be assumed that there is negligible H_2O_2 degradation, which we confirmed by conducting the reaction under N_2 atmosphere (Fig. 5(d)). As anticipated, the reaction rate under N_2 is significantly lower due to limited O_2 availability, indicating that atmospheric O_2 is essential for efficient H_2O_2 photocatalysis.

H_2O_2 photosynthesis may proceed *via* a two-electron, one-step process (O_2/H_2O_2) or a one-electron, two-step process ($O_2/O_2^{\bullet-}/H_2O_2$).

The reaction steps for both mechanisms are as below:

One-step (two electron) reaction mechanism:

$$\text{Oxidation}: \ 2H_2O + 4H^+ \rightarrow O_2 + 4H^+ \quad \text{potential } \textit{vs.} \text{ NHE} = 1.23 \text{ V} \tag{1}$$

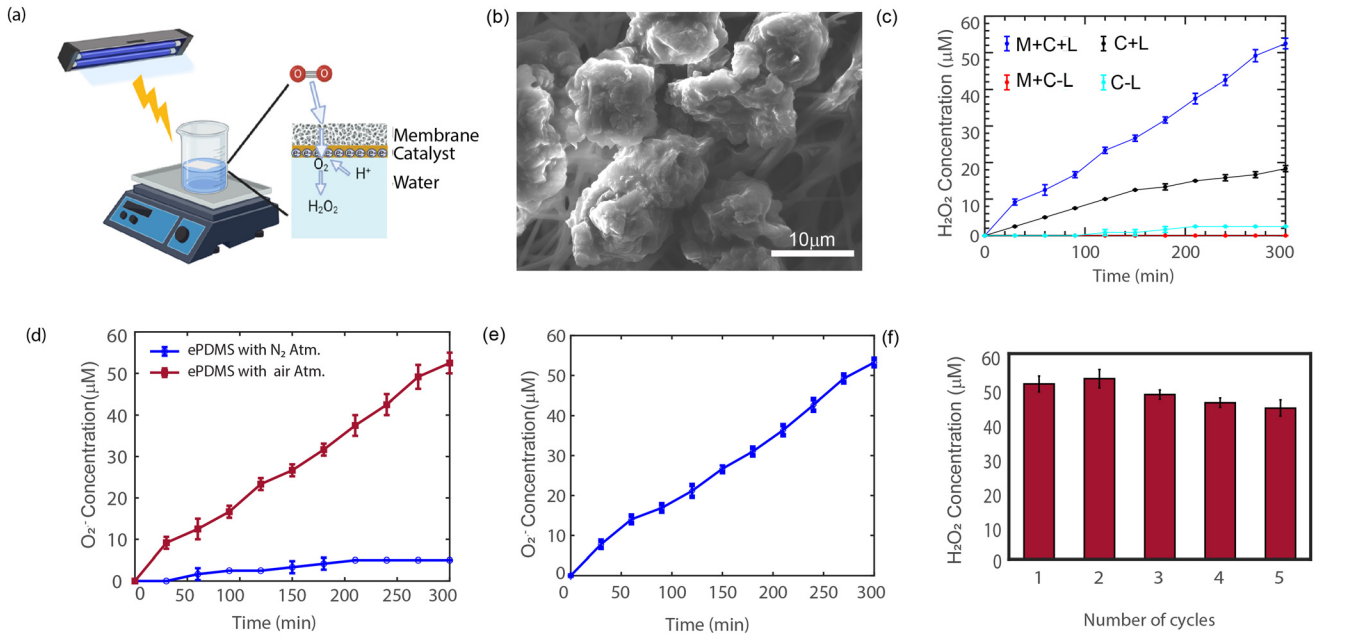

Fig. 5 Photocatalytic conversion of H_2O_2 using C_3N_4-coated ePDMS membranes. (a) General representation of the photocatalytic conversion of H_2O_2 with the catalyst (C_3N_4) coated in the ePDMS membrane, which is then placed on the surface of the water. (b) SEM image of the C_3N_4-coated PDMS membrane. (c) H_2O_2 concentration produced using the C_3N_4-coated PDMS membrane in the presence of light (blue), C_3N_4 solution in water in the presence of light (black curve), C_3N_4 dissolved in water in the absence of light (cyan), and C_3N_4-coated ePDMS membrane in the absence of light (red). (d) H_2O_2 concentration as a function of time for H_2O_2 production in the presence of N_2 and ambient atmosphere. (e) Superoxide radical concentration as a function of time. (f) H_2O_2 concentration for multiple cycles (n = 3).

$$\text{Reduction}: \ O_2 + 2H^+ + 2e^- \rightarrow H_2O_2 \quad \text{potential } vs. \text{ NHE} = 0.68 \text{ V} \tag{2}$$

Two-step (one electron in each step) reaction mechanism:

$$\text{Oxidation}: \ 2H_2O + 4H^+ \rightarrow O_2 + 4H^+ \quad \text{potential } vs. \text{ NHE} = 1.23 \text{ V} \tag{3}$$

$$\text{Reduction}: \ O_2 + e^- \rightarrow O_2^- * \ (1e^- \text{reaction}) \quad \text{potential } vs. \text{ NHE} = -0.33 \text{ V} \tag{4}$$

$$O_2^- * + e^- + 2H^+ \rightarrow H_2O_2 \ (1e^- \text{reaction}) \quad \text{potential } vs. \text{ NHE} = 0.94 \text{ V} \tag{5}$$

We used NBT as a superoxide radical scavenger, which forms monoformazan (MF) upon reaction with superoxide radicals. The absorbance of MF, indicative of superoxide concentration, was measured following the method of Liu *et al.*[49] The result (Fig. 5(e)) suggests that the reaction proceeds *via* the one-electron, two-step pathway ($O_2/O_2^{\bullet -}/H_2O_2$). In this pathway, O_2 first adsorbs onto the catalyst surface, where it undergoes a single electron transfer to form the superoxide anion (O_2^-*). This intermediate is then protonated to generate the hydroperoxyl radical (HOO*), which accepts a second electron and another proton to form H_2O_2. This H_2O_2 desorbs from the catalyst surface into the solution as the final product. The stability of the PDMS-C_3N_4 system was tested over five cycles of H_2O_2 photosynthesis using the same membrane, as shown in Fig. 5(f). After five cycles, the system retained 87% of its initial activity, demonstrating high stability and resistance to photooxidation. The low variability between experiments confirms the reproducibility of H_2O_2 production using the HT-ePDMS membrane system. The consistent performance is attributed to the uniform coating of C_3N_4 on the membrane and the stable oxygen diffusion provided by the porous ePDMS network, which ensures a reliable supply of O_2 to the catalytic sites. The membrane's superhydrophobic and mechanically stable nature further prevents collapse or aggregation during repeated light exposure, supporting sustained activity over multiple cycles. The limitation of the current study is the lack of comprehensive quantitative reproducibility data, owing to the complexity and resource-intensive nature of photocatalytic testing. Future investigations will aim to conduct multiple replicates with rigorous statistical analysis to robustly evaluate the membrane's photocatalytic performance and long-term stability under diverse operational conditions.

4. Conclusion

In summary, the exploration of the electrospinnable PDMS polymer, with its untapped potential and functional property

changes, has opened new research possibilities and paved the way for novel applications. This study establishes a unique ePDMS membrane platform that combines a sequential PMMA reduction strategy, solvent-responsive shrinkage, and asymmetric gold sputtering to achieve programmable folding, trapping, and leak sealing. In addition, using the same membrane as an oxygen-permeable support for H_2O_2 photocatalysis represents, to our knowledge, a previously unreported function for electrospun PDMS systems, underscoring the distinctiveness and versatility of the proposed design. We have successfully electrospun a superhydrophobic PDMS membrane, accompanied by the carrier polymer PMMA, and have effectively removed the majority of the PMMA through intermittent heat treatment following the formation of a 3D membrane network. We observed some shrinkage behavior of the ePDMS membrane in solvents such as IPA and EtOH, which we harnessed for functional applications such as membranous traps and leakage prevention. We achieved this by tuning the permeability of the ePDMS membrane through gold sputtering of various thicknesses and times. These initial insights may be pivotal for future research in the biomedical, sensor, electronic, and soft robotics fields. Additionally, we successfully demonstrated that these membranes can serve as functional platforms for photocatalytic conversion reactions. The ePDMS membranes acted as oxygen diffusion membranes, obviating the need for external oxygen purging, which is critical for perfect catalytic reactions. Further research should focus on optimizing the ePDMS membranes for specific applications, such as controlled fluid release systems, leak-proof barriers, and enhanced oxygen diffusion in catalytic reactions. This sequential heat-treatment strategy, combined with solvent-induced actuation and gold sputtering, establishes a novel, multifunctional platform that extends the conventional use of electrospun PDMS membranes. Their superhydrophobic nature, combined with flexibility and mechanical response to solvents, positions them for use in medical devices, environmental filtration, and industrial applications. Detailed studies will be crucial to refining their performance in these specialized fields.

Author contributions

R. I. R. and G. N. K carried out the ePDMS fabrication and shrinkage experiments, A. T. carried out the catalysis experiments, R. I. R., P. M., S. N. R. and S. D. G. conceived the idea and planned the experiments. S. N. R., P. M., and S. D. G. supervised the work. All the authors contributed to data analysis, interpretation, and manuscript preparation.

Conflicts of interest

The authors declare that they have no known competing financial interests or personal relationships that could have appeared to influence the work reported in this paper.

Abbreviations

ePDMS	Electrospun polydimethylsiloxane
PMMA	Polymethyl methacrylate
THF	Tetrahydrofuran
DMF	Dimethylformamide
HT-ePDMS	Heat-treated electrospun polydimethylsiloxane
AS-ePDMS	As-spun electrospun polydimethylsiloxane
IPA	Isopropyl alcohol
EtOH	Ethanol
SEM	Scanning electron microscopy
τ (tau)	Decay time constant
hr	Hours
PTFE	Polytetrafluoroethylene
FLAP F	Fully gold-sputtered membrane (one side)
FLAP H	Partially gold-sputtered membrane with unsputtered center
3D	Three-dimensional
R6G	Rhodamine 6G
NBT	Nitro blue tetrazolium chloride
MF	Monoformazan
mpg-C_3N_4	Mesoporous graphitic carbon nitride
C_3N_4	Graphitic carbon nitride
M + C + L	Membrane + catalyst + light (photocatalytic setup)
C + L	Catalyst + light (no membrane control)
M + C − L	Membrane + catalyst (no light control)
C–L	Catalyst only (no membrane, no light control)
CQDs	Carbon quantum dots
PNIPAAm	Poly(*N*-isopropylacrylamide)
PEb-PEO	Polyethylene-*b*-ethylene oxide
HEK-293T cells	Human embryonic kidney 293T cells
PLGA	Polylactic-*co*-glycolic acid

Data availability

The data supporting this article have been included as part of the supplementary information (SI). Supplementary information: Wiley Online Library or from the author. See DOI: https://doi.org/10.1039/d5lp00354g.

Acknowledgements

The authors, S. N. R. and S. D.-G., would like to acknowledge funding from the SOCH grant (IITH/BME/F110/SOCH4) for financial support of this project. S.D.-G. would also like to acknowledge funding from Technology Development Grant (TDG/IITH/F199/2024-25/TDG-08) supported by IIT Hyderabad. The authors would also like to acknowledge Prime Ministers Research Fellowship (PMRF) funding for their financial support.

References

1 N. Shehata, M. A. Abdelkareem, E. T. Sayed, D. E. Egirani and A. W. Opukumo, in *Encyclopedia of Smart Materials*, Elsevier, 2022, pp. 288–299.
2 A. Liguori, S. Pandini, C. Rinoldi, N. Zaccheroni, F. Pierini, M. L. Focarete and C. Gualandi, Thermoactive Smart Electrospun Nanofibers, *Macromol. Rapid Commun.*, 2022, **43**, 2100694.
3 M. J. Silva, P. Alves, J. Gomes, R. C. Martins and P. Ferreira, Optimisation of P25/PDMS supported catalysts preparation for the photocatalytic oxidation of parabens, *J. Environ. Chem. Eng.*, 2023, **11**, 110610.
4 X. Chen, J. Wang, J. Zhang, H. Lin, M. Tian, M. Li and Y. Tian, Development and application of electrospun fiber-based multifunctional sensors, *Chem. Eng. J.*, 2024, **486**, 150204.
5 S. Chen, Y. Xie, K. Ma, Z. Wei, X. Ran, X. Fu, C. Zhang and C. Zhao, Electrospun nanofibrous membranes meet antibacterial nanomaterials: From preparation strategies to biomedical applications, *Bioact. Mater.*, 2024, **42**, 478–518.
6 Y. Tang, Z. Cai, X. Sun, C. Chong, X. Yan, M. Li and J. Xu, Electrospun Nanofiber-Based Membranes for Water Treatment, *Polymers*, 2022, **14**, 2004.
7 B. J. Deka, E. J. Lee, J. Guo, J. Kharraz and A. K. An, Electrospun Nanofiber Membranes Incorporating PDMS-Aerogel Superhydrophobic Coating with Enhanced Flux and Improved Antiwettability in Membrane Distillation, *Environ. Sci. Technol.*, 2019, **53**, 4948–4958.
8 S. Zheng, X. Wang, W. Li, Z. Liu, Q. Li and F. Yan, Pressure-stamped stretchable electronics using a nanofibre membrane containing semi-embedded liquid metal particles, *Nat. Electron.*, 2024, **7**, 576–585.
9 L. F. Ren, C. Liu, Y. Xu, X. Zhang, J. Shao and Y. He, High-performance electrospinning-phase inversion composite PDMS membrane for extractive membrane bioreactor: Fabrication, characterization, optimization and application, *J. Membr. Sci.*, 2020, **597**, 117624.
10 V. Fasano, R. Laurita, M. Moffa, C. Gualandi, V. Colombo, M. Gherardi, E. Zussman, G. Vasilyev, L. Persano, A. Camposeo, M. L. Focarete and D. Pisignano, Enhanced Electrospinning of Active Organic Fibers by Plasma Treatment on Conjugated Polymer Solutions, *ACS Appl. Mater. Interfaces*, 2020, **12**(23), 26320–26329.
11 J. Xue, T. Wu, Y. Dai and Y. Xia, Electrospinning and electrospun nanofibers: Methods, materials, and applications, *Chem. Rev.*, 2019, **119**(8), 5298–5415.
12 A. I. Aghmiuni, A. Ghadi, E. Azmoun, N. Kalantari, I. Mohammadi and H. H. Kordmahaleh, in *Electrospinning - Material Technology of the Future*, 2022, p. 144.
13 C. Yuan, S. Jin, J. Wei, J. Huang, C. Liu, X. Lei, Y. Zuo, J. Li and Y. Li, The shrinking behaviour, mechanism and anti-shrinkage resolution of an electrospun PLGA membrane, *J. Mater. Chem. B*, 2021, **9**(29), 5861–5868.
14 F. Fang, H. Wang, W. M. Huang, Y. Chen, N. Cai, X. Chen and X. Chen, Stimulus-responsive shrinkage in electrospun membranes: Fundamentals and control, *Micromachines*, 1, **12**(8), 920.
15 B. Gautam, M. R. Huang, S. A. Ali, A. L. Yan, H. H. Yu and J. T. Chen, Smart Thermoresponsive Electrospun Nanofibers with On-Demand Release of Carbon Quantum Dots for Cellular Uptake, *ACS Appl. Mater. Interfaces*, 2022, **14**, 40322–40330.
16 F. F. P. da Costa, E. S. Araújo, M. L. F. Nascimento and H. P. De Oliveira, Electrospun Fibers of Enteric Polymer for Controlled Drug Delivery, *Int. J. Polym. Sci.*, 2015, 902365.
17 Q. Gao, B. A. F. Kopera, J. Zhu, X. Liao, C. Gao, M. Retsch, S. Agarwal and A. Greiner, Breathable and Flexible Polymer Membranes with Mechanoresponsive Electric Resistance, *Adv. Funct. Mater.*, 2020, **30**, 1907555.
18 R. Walden, I. Aazem, S. Hinder, B. Brennan, A. Goswami, G. McGranaghan and S. C. Pillai, Parametric optimisation of PDMS/PMMA nanofibers prepared using emulsion electrospinning technique, *Results Mater.*, 2024, **22**, 100576.
19 D. Yang, X. Liu, Y. Jin, Y. Zhu, D. Zeng, X. Jiang and H. Ma, Electrospinning of poly(dimethylsiloxane)/poly(methyl methacrylate) nanofibrous membrane: Fabrication and application in protein microarrays, *Biomacromolecules*, 2009, **10**, 3335–3340.
20 S. Pulipaka, A. K. S. Koushik, N. Boni, M. Deepa and P. Meduri, Tin disulfide based ternary composites for visible light driven photoelectrochemical water splitting, *Int. J. Hydrogen Energy*, 2019, **44**, 11584–11592.
21 L. F. Ren, F. Xia, J. Shao, X. Zhang and J. Li, Experimental investigation of the effect of electrospinning parameters on properties of superhydrophobic PDMS/PMMA membrane and its application in membrane distillation, *Desalination*, 2017, **404**, 155–166.
22 S. Chaurasia, U. Rao, A. K. Mishra, C. D. Sijoy and V. Mishra, Raman spectroscopy of poly (methyl methacrylate) under laser shock and static compression, *J. Raman Spectrosc.*, 2020, **51**, 860–870.
23 D. C. Kang, T. Y. Wang, D. S. Lin, Y. S. Cheng and C. W. Huang, PDMS with porous PMMA dual-layer coating for passive daytime radiative cooling, *Sol. Energy Mater. Sol. Cells*, 2025, **282**, 113380.
24 A. S. Cruz-Félix, A. Santiago-Alvarado, J. Márquez-García and J. González-García, PDMS samples characterization with variations of synthesis parameters for tunable optics applications, *Heliyon*, 2020, **6**, e03064.
25 S. Hassanpour-Tamrin, A. Sanati-Nezhad and A. Sen, A simple and low-cost approach for irreversible bonding of polymethylmethacrylate and polydimethylsiloxane at room temperature for high-pressure hybrid microfluidics, *Sci. Rep.*, 2021, **11**, 4821.
26 P. Wang, H. Lv, X. Cao, Y. Liu and D. G. Yu, Recent Progress of the Preparation and Application of Electrospun Porous Nanofibers, *Polymers*, 2023, **15**(4), 921.
27 X. Chen, W. Hung, G. Liu, K. Lee and W. Jin, PDMS mixed–matrix membranes with molecular fillers via reactive incorporation and their application for bio–butanol

recovery from aqueous solution, *J. Polym. Sci.*, 2020, **58**, 2634–2643.
28 N. Lu, Z. Hu, F. Wang, L. Yan, H. Sun, Z. Zhu, W. Liang and A. Li, Superwetting Electrospun PDMS/PMMA Membrane for PM2.5Capture and Microdroplet Transfer, *Langmuir*, 2021, **37**, 2972–12980.
29 H. Liang, M. Liu, D. Sun, D. Yue, Y. Ge, F. Li, M. Shi and Z. Shi, Asymmetric PDMS/PVDF Pervaporation Membrane for Separation of Ethanol/Water System, *ChemistrySelect*, 2024, **9**, e202401075.
30 R. Demoor and J. P. Tomba, Permeability in barrier membranes: Comparison between experiments, direct calculations, and analytical models, *Polym. Eng. Sci.*, 2023, **63**, 2385–2396.
31 J. Liu, Y. Sun, X. Zhou, X. Li, M. Kappl, W. Steffen and H. J. Butt, One-Step Synthesis of a Durable and Liquid-Repellent Poly(dimethylsiloxane) Coating, *Adv. Mater.*, 2021, **33**, 2100237.
32 Y. Li, X. Liu, J. Liu and S. Xiang, Fabrication and characterization study of ultrathin multi-walled carbon nanotubes/polydimethylsiloxane composite membranes for strain sensing application, *Polym. Compos.*, 2022, **43**, 5390–5403.
33 C. Sutthiwanjampa, S. Hong, W. J. Kim, S. H. Kang and H. Park, Hydrophilic Modification Strategies to Enhance the Surface Biocompatibility of Poly(dimethylsiloxane)-Based Biomaterials for Medical Applications, *Adv. Mater. Interfaces*, 2023, **10**, 2202333.
34 M. M. Keshtiban, M. M. Zand, A. Ebadi and Z. Azizi, PDMS-based porous membrane for medical applications: design, development, and fabrication, *Biomed. Mater.*, 2023, **18**, 045012.
35 L. F. Ren, F. Xia, J. Shao, X. Zhang and J. Li, Experimental investigation of the effect of electrospinning parameters on properties of superhydrophobic PDMS/PMMA membrane and its application in membrane distillation, *Desalination*, 2017, **404**, 155–166.
36 S. Nauman, G. Lubineau and H. F. Alharbi, Post processing strategies for the enhancement of mechanical properties of enms (Electrospun nanofibrous membranes), *Membranes*, 2021, **11**(1), 39.
37 D. B. Menezes, A. Reyer, A. Benisek, E. Dachs, C. Pruner and M. Musso, Raman spectroscopic insights into the glass transition of poly(methyl methacrylate), *Phys. Chem. Chem. Phys.*, 2021, **23**, 1649–1665.
38 A. Ahmad, S. H. Li and Z. P. Zhao, Insight of organic molecule dissolution and diffusion in cross-linked polydimethylsiloxane using molecular simulation, *J. Membr. Sci.*, 2021, **620**, 118863.
39 F. Kadirkhan, P. S. Goh, A. F. Ismail, W. N. F. Wan Mustapa, M. H. M. Halim, W. K. Soh and S. Y. Yeo, Recent Advances of Polymeric Membranes in Tackling Plasticization and Aging for Practical Industrial CO2/CH4 Applications—A Review, *Membranes*, 2022, **12**(1), 71.
40 S. U. Patel, G. M. Manzo, S. U. Patel, P. S. Kulkarni and G. G. Chase, Permeability of electrospun superhydrophobic nanofiber mats, *J. Nanotechnol.*, 2012, 483976.
41 B. Yan, Y. Zhang, Z. Li, P. Zhou and Y. Mao, Electrospun nanofibrous membrane for biomedical application, *J. Mater. Sci.*, 2022, **4**, 172.
42 I. Apsite, G. Stoychev, W. Zhang, D. Jehnichen, J. Xie and L. Ionov, Porous Stimuli-Responsive Self-Folding Electrospun Mats for 4D Biofabrication, *Biomacromolecules*, 2017, **18**(10), 3178–3184.
43 M. J. Airaghi Leccardi, B. X. E. Desbiolles, A. Y. Haddad, B. C. Joy, C. Song and D. Sarkar, Light-induced rolling of azobenzene polymer thin films for wrapping subcellular neuronal structures, *Commun. Chem.*, 2024, **7**, 249.
44 J. Kim and X. Jia, Flexible multimaterial fibers in modern biomedical applications, *Natl. Sci. Rev.*, 2024, **11**, nwae333.
45 L. Nie, H. Chen, J. Wang, Y. Yang and C. Fang, Enhanced Visible-Light H_2O_2 Production over Pt/g-C3N4 Schottky Junction Photocatalyst, *Inorg. Chem.*, 2024, **63**, 4770–4782.
46 S. Zhao, Y. Yang, F. Bi, Y. Chen, M. Wu, X. Zhang and G. Wang, Oxygen vacancies in the catalyst: Efficient degradation of gaseous pollutants, *Chem. Eng. J.*, 2023, **454**, 140376.
47 L. Chen, S. Li, Z. Yang, C. Chen, C. Chu and B. Chen, Enhanced photocatalytic hydrogen peroxide production at a solid-liquid-air interface via microenvironment engineering, *Appl. Catal., B*, 2022, **305**, 121066.
48 S. Thakur, T. Kshetri, N. H. Kim and J. H. Lee, Sunlight-driven sustainable production of hydrogen peroxide using a CdS–graphene hybrid photocatalyst, *J. Catal.*, 2017, **345**, 78–86.
49 R. H. Liu, S. Y. Fu, H. Y. Zhan and L. A. Lucia, General spectroscopic protocol to obtain the concentration of the superoxide anion radical, *Ind. Eng. Chem. Res.*, 2009, **48**, 9331–9334.